applied sciences

MDPI

Article

Effects of Pyrolysis and Ball-Milling on the Physicochemical and Rhodamine B Removal Characteristics of Rice-Bran-Derived Biochar

Da-Young Kim and Gyeong-Bok Jung *

Department of Physics Education, Chosun University, Gwangju 61452, Republic of Korea
* Correspondence: gbjung@chosun.ac.kr; Tel.: +82-062-2307375

Abstract: Biochar has attracted considerable attention in numerous industrial and environmental applications because of its advantageous properties. Pyrolysis, a cost-effective and eco-friendly engineering technique for improving biochar's physicochemical and adsorption properties, is important in a variety of environmental applications. The effect of pyrolysis temperature and ball-milling time on the physicochemical properties of biochar derived from rice bran was investigated in this study, and its effectiveness in the aqueous removal of rhodamine B (RhB) dye was evaluated. The biochar was prepared by pyrolyzing rice bran at various temperatures, i.e., 400, 500, 600, and 700 °C (RB 400, RB 500, RB 600, and RB 700, respectively). In addition, in order to investigate the effect of the ball-milling time on the RB 600 biochar, it was milled for 30, 60, 120, 180, and 240 min. The surfaces of the raw material and biochar exhibited honeycomb-like pores and a layered structure. The biochar structure shrank, became fragile, and cracked as the pyrolysis temperature increased. After ball milling, the honeycomb-like pores and layered structure of the pristine biochar were transformed into irregular particles. The particle size decreased as milling time increased. Furthermore, the physicochemical properties of ball-milled biochar were superior to those of pristine biochar. According to the Raman spectral analysis, the I_D/I_G ratio decreased as the pyrolysis temperature and the milling time increased, indicating a decreased disorder and an increased graphitization in the biochar. The efficiency of RhB removal increased as the pyrolysis temperature and ball-milling time increased, and up to 82% of RhB was removed from 50 mg of biochar milled for 180 min at 600 °C.

Keywords: biochar; high-energy ball-milling; pyrolysis; adsorption; Raman spectroscopy

Citation: Kim, D.-Y.; Jung, G.-B. Effects of Pyrolysis and Ball-Milling on the Physicochemical and Rhodamine B Removal Characteristics of Rice-Bran-Derived Biochar. *Appl. Sci.* **2023**, *13*, 4288. https://doi.org/10.3390/app13074288

Academic Editor: Gerhard Soja

Received: 16 February 2023
Revised: 25 March 2023
Accepted: 27 March 2023
Published: 28 March 2023

1. Introduction

Environmental pollution from heavy metals or dyes has been progressively worsening, owing to rapid industrial growth, and has now become a worldwide issue [1]. Therefore, eco-friendly, cost-effective, and high-efficiency adsorbents for heavy metal- or dye-contaminated water are urgently required. Recently, biochar has attracted considerable attention for environmental protection, owing to its unique physicochemical properties [2–4]. Biochar is a carbonaceous material made by pyrolyzing biomass in the absence of oxygen, and has garnered a significant interest as a less toxic, environmentally friendly, and inexpensive material [5–9]. Additionally, biochar has the advantages of a high specific surface area, a well-developed mesoporous structure, enriched surface functional groups, and mineral components, making it an excellent adsorbent for removing contaminants from aqueous solutions. Compared to traditional activated carbon, biochar is a new cost-effective and efficient sorbent candidate. A higher temperature is required for the production of activated carbon, whereas the production of biochar, which is derived from agricultural biomass and solid wastes, is cheaper and requires less energy [10–12]. Previous studies have shown that biochar is incredibly effective at removing various organic and inorganic pollutants, such as heavy metals, dyes, and polycyclic aromatic hydrocarbons [13–16]. Hsieh et al. used modified biochar to remove malachite green from polluted aqueous

environments [17]. Among the various biochars, rice-bran-derived biochar has been widely studied as a raw material for biochar synthesis for use as an adsorbent material, due to its chemical stability and local availability [18–20].

The physical and chemical properties of biochar depend on several factors related to the pyrolysis temperature and the milling process. Ball milling is a mechanochemical process that utilizes mechanical energy to induce chemical and structural changes in materials, and is now considered a green technology for pristine biochar modification [21,22]. Xu et al. studied mesoporous ball-milled Fe-loaded biochar for enhanced sorption of reactive red [23]. Pyrolysis is the thermochemical conversion of agricultural organic waste, and the pyrolysis temperature is related to the biochar yield and its physicochemical characteristics [24–26].

However, the effects of pyrolysis and ball milling on the physicochemical and adsorption properties of rice-bran-derived biochar remain unexplored. Rice bran is a major agricultural waste in Korea, and the potential applications of this biomass are currently under study. Thus, in the present study, we investigated the effect of pyrolysis temperature and ball-milling time on the physicochemical properties of rice-bran-derived biochar. Moreover, we demonstrated the effects of pyrolysis temperature, ball-milling time, biochar dose, and contact reaction time on the Rhodamine B (RhB) removal efficiency of the rice-bran-derived biochar. RhB is widely used in textile production and paper printing, as well as in the biological, analytical and optical sciences [27,28]. RhB can cause burning of the eyes and throat, chest pain, cough, and headache in humans [29,30]. However, RhB is a common contaminant in waste water; therefore, removing RhB from waste water is critical not only for fundamental studies but also for aquatic life and human health.

2. Materials and Methods

2.1. Synthesis of the Rice Brain Biochar

Rice bran was obtained from a local rice mill facility in Seokgok, Republic of Korea. The rice bran was washed with deionized water and dried for 48 h at 80 °C. To remove ash and non-water-soluble substances from the samples, the rice bran was rinsed several times with 0.1 M HCl in a beaker, subsequently washed by deionized water, and then dried for 24 h at 80 °C. Next, we pyrolyzed the rice bran. The pyrolysis experiments were carried out in a muffle furnace under a nitrogen atmosphere. Subsequently, 5 g samples of the dried raw bran were placed in the furnace and heated at a rate of 5 °C/min from room temperature to 400, 500, 600, and 700 °C for 1 h under a 3000 cc/min nitrogen (inert) gas flow. The samples were then cooled to room temperature. The rice bran biochar samples obtained at various pyrolysis temperatures were labeled as RB400, RB500, RB600, and RB700, respectively.

2.2. Preparation of the Ball-Milled Biochar

The synthesized rice bran biochar was placed in an 80 mL zirconia jar with 3 mm zirconia balls inside of a planetary ball-mill machine (Pulverisette 6 Fritsch, Idar-Oberstein, Germany) and milled at 300 rpm in ambient air. The weight ratio of the sample to the ball was 50:1. To prevent the biochar and balls from overheating, the biochar was milled for 15 min and then rested for 15 min. In order to investigate the effect of the ball-milling time on the RB600 biochar, it was milled for 30, 60, 120, 180, and 240 min.

2.3. Characterization of the Biochar

To characterize the crystal structures of the biochar samples, X-ray diffraction (XRD, PANalytical, X'pert PRO MPD) analysis was performed in the $2\theta = 10°–90°$ measurement with Cu K_α radiation ($\lambda = 1.54060$ Å) at a scanning rate of 0.02°/s. The acceleration voltage and current were set to 40 kV and 30 mA, respectively. The surface morphology of the biochar was analyzed by field-emission scanning electron microscopy (FE-SEM; S-4800 Hitachi) at 15 kV. Fourier transform infrared (FTIR) spectroscopy was used to examine the surface-functional groups in the biochar samples. (FT/IR-4200 spectrometer, JASCO,

Japan). The samples were measured using a KBr pellet in the 400–4000 cm^{-1} range. A 785-nm diode laser source-equipped XperRam F1.4 system (Nanobase Inc., Seoul, Korea) was used to record the Raman spectra in the 800–1800 cm^{-1} range. The particle size and zeta potential of the biochar samples were measured by dynamic light scattering (DLS) using the same instrument and by nanoparticle tracking analysis (Zetasizer Nano ZSP, Malvern Worcestershire, UK).

2.4. Removal of RhB

In order to investigate the effects of different pyrolysis temperatures and ball-milling times on the RhB removal efficiency of the biochar samples, 50 mg samples of the biochar were mixed with 50 mL of RhB for 10 min. An RhB solution (10 μM) was obtained by solubilizing RhB in deionized water. The effect of the biochar doses (10, 20, 30, 40, 50, 60, 70, 80, 90, and 100 mg) on the RhB solution (10 μM) was studied using a sample with a pyrolysis temperature of 600 °C and a ball-milling time of 180 min. The contact reaction time was 10 min. The effect of contact reaction times (0, 4, 8, 12, 16, and 20 min) on the RhB solution (10 μM) was investigated using a sample with a pyrolysis temperature of 600 °C and a ball-milling time of 180 min. The biochar dose was 50 mg. In all of the experiments, a mechanical shaker at room temperature was used to shake the mixtures at a constant rate of 100 rpm. After the removal test, the withdrawn samples were separated twice by centrifugation at 8000 rpm for 5 min. The final concentration of the residual RhB solution was determined using a fluorescence spectrometer (Fluormax-4; Horiba, Japan) at a maximum wavelength of 576 nm. The removal percentage (R%) was calculated as follows [31]:

$$R\% = \frac{(C_0 - C_e)}{C_0} \times 100 \quad (1)$$

where C_0 (mg L^{-1}) and C_e (mg L^{-1}) are the initial and equilibrium RhB concentrations, respectively.

3. Results and Discussion

3.1. Biochar Characterization

The surface morphology and particle size of the pristine and ball-milled biochar samples were characterized using SEM. Figure 1a shows the SEM images of the raw and biochar samples obtained at various pyrolysis temperatures of 400, 500, 600, and 700 °C (RB 400, RB 500, RB 600, and RB 700). The surface morphologies of the raw and biochar samples show honeycomb-like pores and a layered structure. As the pyrolysis temperature increases, the structure of the biochar shrinks. Furthermore, owing to their thin walls, the structures appear fragile and cracked. Figure 1b presents the SEM images of the biochar sample RB600 milled for 30, 60, 120, 180, and 240 min. After ball milling, the honeycomb-like pores and layered structure of the pristine biochar change to irregular particles. The particle size decreases with increased milling time. DLS measurements were also performed to investigate the particle size distribution. As shown in Figure 1c, the particle size decreases with increased milling time, and after 180 min, the particle size is approximately 350 nm. This result is consistent with the SEM image shown in Figure 1b.

XRD was performed in order to characterize the crystalline structures. Figure 2a displays the XRD patterns of the biochar samples at different pyrolysis temperatures (400, 500, 600, and 700 °C). As shown in Figure 2a, the biochar samples' XRD spectra show two broad peaks centered at $2\theta = 23^\circ$ and 43°, which correspond to the (002) and (100) planes of graphitic carbon materials, respectively. No crystalline structure is detected; that is, there is no sharp peak, implying that the biochar structures are completely amorphous. Figure 2b shows the XRD patterns of the RB600 biochar ball milled for different times (30, 60, 120, 180, and 240 min). The XRD spectra of all biochar samples show similar trends, as shown in Figure 2b, with two broad peaks at $2\theta \approx 23^\circ$ and 43°.

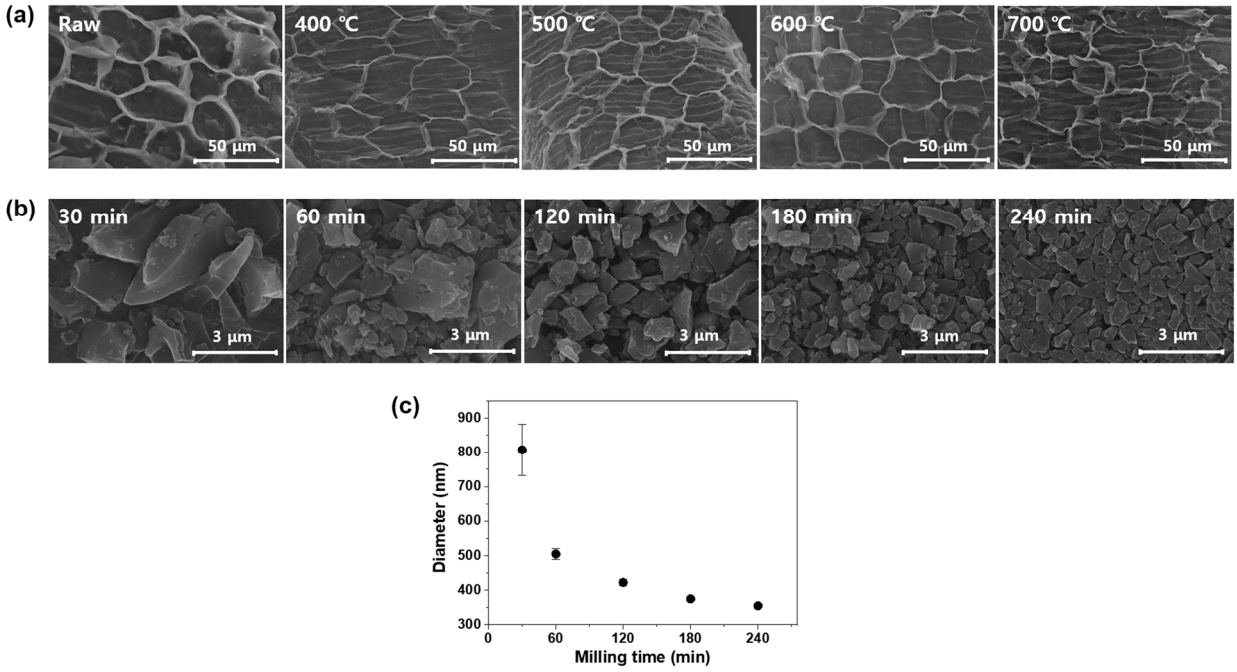

Figure 1. SEM images of the biochar samples obtained at different (**a**) pyrolysis temperatures and (**b**) ball-milling times. (**c**) Particle size distribution with respect to ball-milling times.

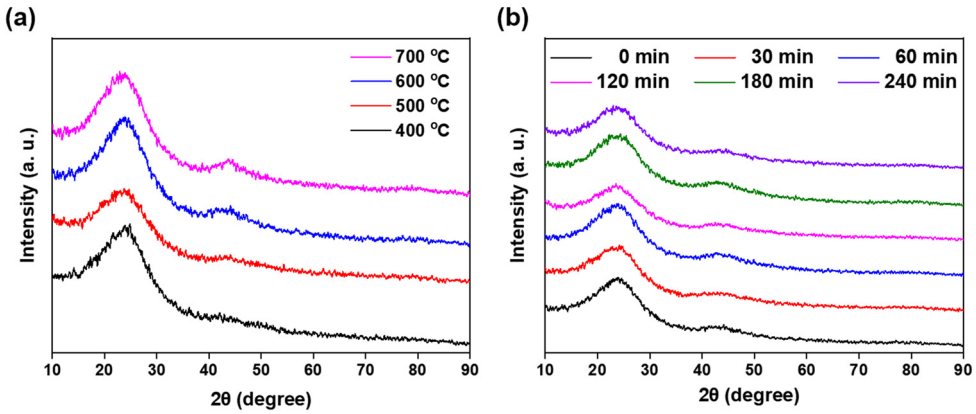

Figure 2. XRD patterns of the biochar samples obtained at different (**a**) pyrolysis temperatures and (**b**) ball-milling times.

Raman spectroscopy is an important characterization technique for highly disordered carbonaceous materials, such as biochar, owing to its sensitivity to molecular structures with a short-range order. Figure 3 shows the deconvoluted and fitted Raman peaks of the biochar samples at different pyrolysis temperatures and milling times; the black circle and blue line are the original raw data and fitted data, respectively. The D and G bands are depicted in red and green, respectively. As shown in Figure 3a, the Raman spectra of the biochar sample exhibit two broad bands at approximately 1330 and 1580 cm^{-1}, which are defined as the D and G peaks, respectively. The D band at 1330 cm^{-1} is related to the disordered and defective structure of the biochar [32], and the G band at 1580 cm^{-1} arises from the in-plane vibrations of the sp^2 graphitic structure of the biochar [33]. The broad D and G bands are deconvoluted into two components. The intensity ratio, I_D/I_G, and full width at half maximum (FWHM) are used to determine the defect density and degree of crystallinity [34], respectively, which can indicate the quality of the biochar. A low I_D/I_G ratio and narrow FWHM suggest a high biochar quality. As the pyrolysis temperature increases from 400 °C to 700 °C, the I_D/I_G ratio decreases (2.70, 2.05, 1.76,

and 1.82) (Figure 3a). This result indicates that the disorder decreases and graphitization increases with increasied pyrolysis temperature. The FWHM of the biochar becomes narrower with increased pyrolysis temperature, indicating that the crystalline quality of the biochar increases with increased pyrolysis temperature. Further, the I_D/I_G ratio slightly decreases (1.81, 1.75, 1.66, 1.68, 1.71, and 1.77) as the milling time increases (0, 30, 60, 120, 180, and 240 min, respectively). This behavior indicates that as the milling time increases, the disorder and defective structure of the biochar decreases. The FWHM of the biochar narrows with increased milling time. However, the FWHM of the biochar milled for 240 min is wider than that of the other samples, indicating that this biochar has a low crystalline quality.

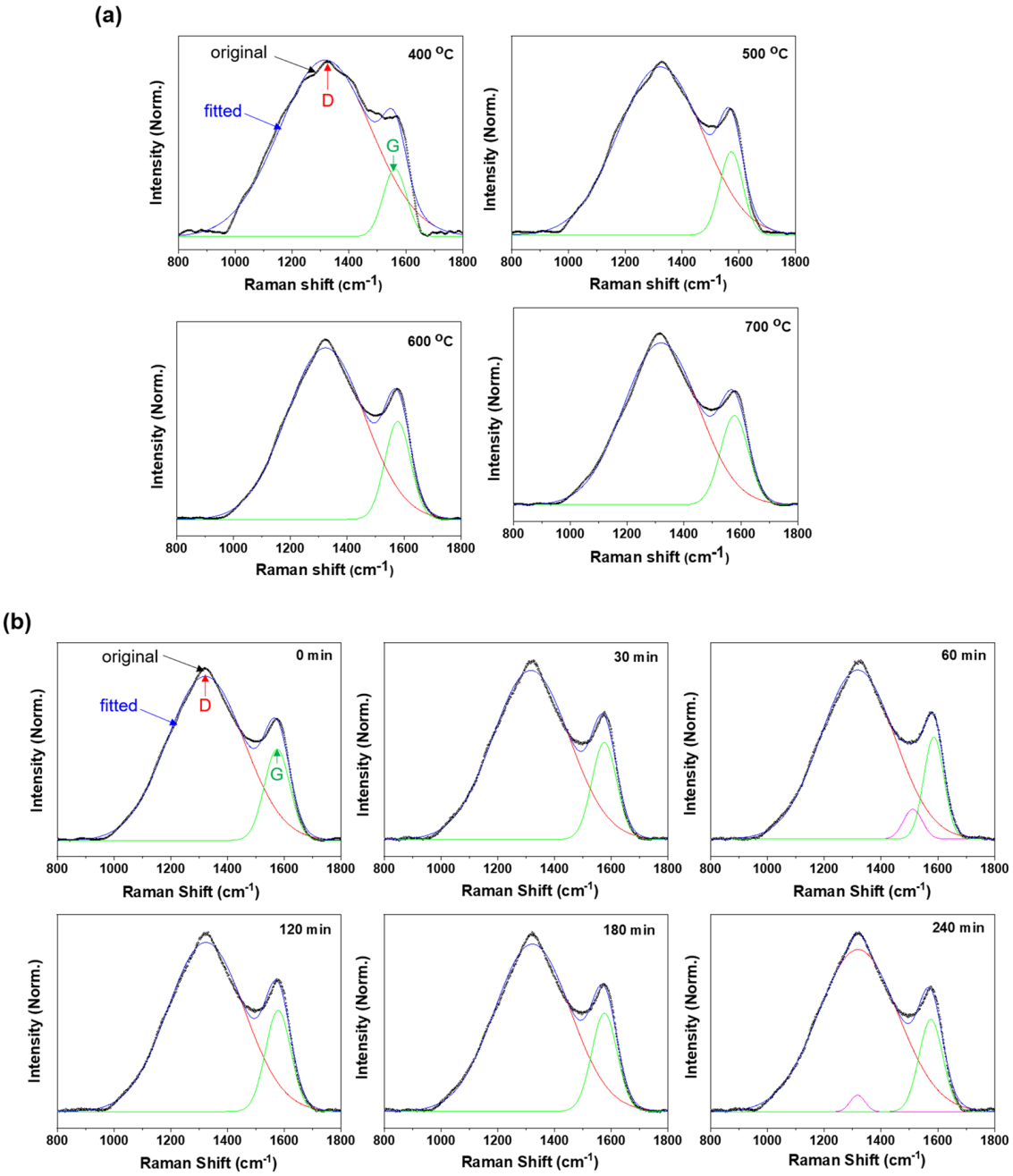

Figure 3. Deconvoluted and fitted Raman spectra of the biochar samples obtained at different (**a**) pyrolysis temperatures and (**b**) ball-milling times. The black circle and blue line are the original raw data and fitted data, respectively. The D and G bands are depicted in red and green, respectively.

Figure 4 shows the FTIR spectra of the biochar samples at different pyrolysis temperatures and milling times. Evidently, the FTIR spectra of all the biochar samples show almost similar trends. The band at 1070 cm^{-1} is attributed to the stretching vibration of C-O, and the peak at 1651 cm^{-1} corresponds to the stretching vibration of C=C. The O-H stretching mode is associated with the broad band at 3416 cm^{-1} [35].

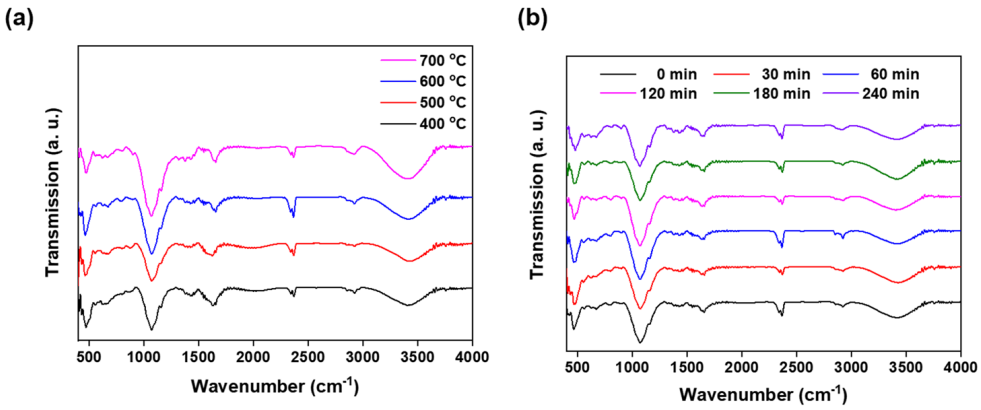

Figure 4. FTIR spectra of the biochar samples at different (**a**) pyrolysis temperatures and (**b**) ball-milling times.

The biochar samples produced at different pyrolysis temperatures and milling times show significantly different morphological structures, resulting in changes in the electrical potentials on their surfaces. The surface electrical potential of the biochar samples was investigated using a zeta potential analyzer. Zeta potential is a crucial factor for determining the effect of particles in a suspension on particle agglomeration, sedimentation, and interactions [36].

Figure 5a shows the zeta potentials of the biochar surfaces at different pyrolysis temperatures. The zeta potential gradually decreases with increased pyrolysis temperature. This result indicates that the negative charge of the biochar surface gradually increases, resulting in a strong electronegativity. Figure 5b shows the zeta potential of the biochar surface after different milling times, indicating that the zeta potential gradually decreases with increased milling time. This result may be related to particle agglomeration, because milling time minimizes particle agglomeration. This result is in good agreement with the SEM images shown in Figure 1b.

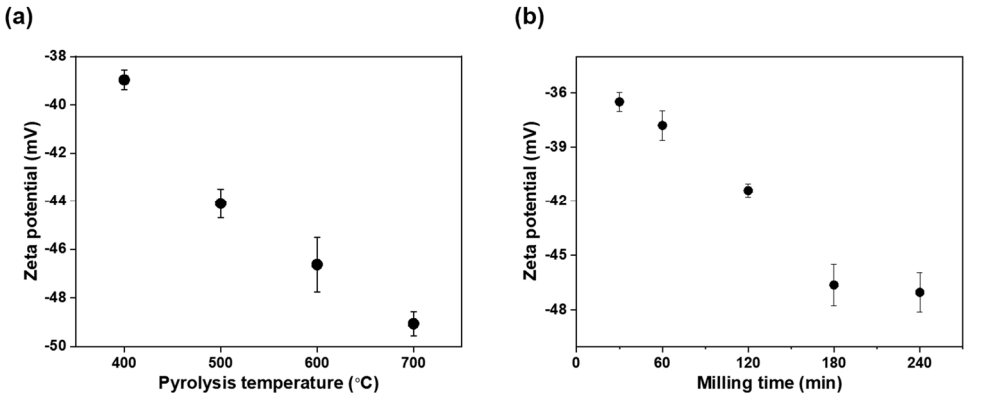

Figure 5. Zeta potentials of the biochar samples at different (**a**) pyrolysis temperatures and (**b**) ball-milling times.

3.2. Removal of RhB

Applying the optimum conditions for biochar is important for its cost-effective application in contaminant removal. Thus, we investigated the effects of pyrolysis temperature,

milling time, adsorbent dosage, and contact reaction time on RhB removal using biochar. Figure 6 shows the photoluminescence spectra and the RhB removal efficiency at different pyrolysis temperatures, milling times, adsorbent dosages, and contact reaction times; the inset of the graph displays a photograph of the corresponding stage. The RhB removal efficiency is calculated at a maximum wavelength of 576 nm by Equation (1). The effect of the pyrolysis temperature on RhB was investigated using a biochar concentration of 50 mg. The contact reaction time was fixed at 10 min. Evidently, the removal percentage increases rapidly as the pyrolysis temperature increases, and a maximum percentage removal of 82% is observed for RhB using RB600 (Figure 6a). In the remaining experiments, we evaluated the RhB removal characteristics of the biochar using RB600. Figure 6b shows the RhB removal efficiency of the biochar for different milling times. The removal efficiency increases with increased milling time; the removal efficiencies of the unmilled and 180-min milled biochar samples are 5% and 82%, respectively. This finding suggests that ball milling is an excellent engineering method for improving organic pollutant removal characteristics.

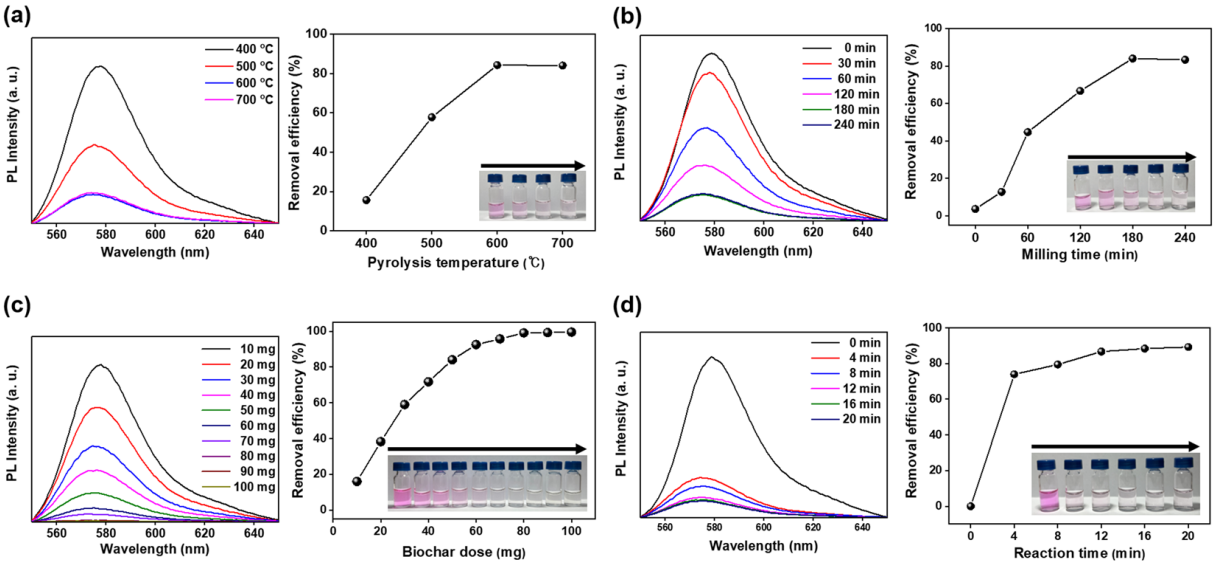

Figure 6. Photoluminescence spectra and removal efficiency of RhB at different (**a**) pyrolytic temperatures, (**b**) ball-milling times, (**c**) biochar doses, and (**d**) contact reaction times. The insets show photographs of the corresponding stage.

Adsorbent dose is a crucial factor in regulating the effectiveness of organic pollutant removal. The effect of biochar dosage on its RhB removal efficiency was investigated in the range of 10–100 mg using RB600 and the 180-min milled biochar sample. Initially, the removal efficiency increases, and the maximum RhB removal is observed at 80 mg (~99%). However, as the biochar dose is increased beyond the optimum dose, the RhB removal efficiency remains almost identical. When the adsorbent dose is increased, the dye molecules and biochar can form agglomerations and clusters, thereby limiting the active binding sites and lowering the overall efficiency [28]. In the biochar adsorption process, the contact reaction time of the dyes is an important factor in the design of adsorption systems. Figure 6d presents the RhB removal efficiencies of the RB600, 180-min milled, and 50 mg of biochar samples at different contact reaction times (0–20 min). At the beginning of the reaction, the removal efficiency rapidly increases with increased reaction time due to the numerous active sites. The maximum RhB removal is observed at 12 min (removal efficiency 82%). As the contact reaction time increases further, the RhB removal efficiencies remain nearly identical.

4. Conclusions

In this study, we demonstrated the characteristics of rice-bran-derived biochar at different pyrolysis temperatures (400, 500, 600, and 700 °C) and ball-milling times (30, 60, 120, 180, and 240 min). The effects of the pyrolysis temperature, ball-milling time, adsorbent amount, and contact reaction time on the RhB removal performance were also investigated. The pyrolysis temperature and ball-milling time had a significant impact on the physicochemical and structural properties of the biochar. The FTIR analysis revealed that all of the biochar samples contained similar functional groups (C-O, C=C, and C-H). With increased pyrolysis temperature, the biochar exhibited a highly ordered aromatic carbon structure. In addition, as the pyrolysis temperature was increased, the RhB removal efficiency increased as well.

When compared to pristine biochar, ball-milled biochar demonstrated improved physicochemical properties, and its RhB removal efficiency was remarkable compared to that of unmilled biochar. Among the samples, the 180-min ball-milled RB600 biochar sample exhibited the highest RhB removal efficiency due to the tiny particle size and high surface area obtained through ball milling and high pyrolysis temperature. These results reveal that the ball-milling technique has a high potential for efficiency improvement and is an environmentally friendly and cost-effective technique for a wide range of environmental applications. In the future, we will further investigate the physicochemical properties of biochar by extending the pyrolysis temperature and ball milling time to enhance the generalizability of this study's findings. In addition, the adsorption kinetics and isotherms of heavy metals and dyes to rice-bran-derived biochar will be studied in detail.

Author Contributions: D.-Y.K.: Methodology, Conceptualization, Data curation, Formal analysis, Visualization. G.-B.J.: Conceptualization, Supervision, Writing—review & editing, Funding acquisition. All authors have read and agreed to the published version of the manuscript.

Funding: This study was supported by the 2021 Research Fund of Chosun University.

Institutional Review Board Statement: Not applicable.

Informed Consent Statement: Not applicable.

Data Availability Statement: Not applicable.

Conflicts of Interest: All authors declare that they have no conflict of interest.

References

1. Bilal, M.; Adeel, M.; Rasheed, T.; Zhao, Y.; Iqbal, H.M.N. Emerging contaminants of high concern and their enzyme-assisted biodegradation—A review. *Environ. Int.* **2019**, *124*, 336–353. [CrossRef]
2. Lu, Y.; Cai, Y.; Zhang, S.; Zhuang, L.; Hu, B.; Wang, S.; Chen, J.; Wang., X. Application of biochar-based photocatalysts for adsorption-(photo) degradation/ reduction of environmental contaminants: Mechanism, challenges and perspective. *Biochar* **2022**, *4*, 45. [CrossRef]
3. Cui, J.; Zhang, F.; Li, H.; Cui, J.; Ren, Y.; Yu, X. Recent Progress in Biochar-Based Photocatalysts for Wastewater Treatment: Synthesis, Mechanisms, and Applications. *Appl. Sci.* **2020**, *10*, 1019. [CrossRef]
4. Zubair, M.; Múazu, N.D.; Jarrah, N.; Blaisi, N.I.; Aziz, H.A.; Al-Harthi, M.A. Adsorption Behavior and Mechanism of Methylene Blue, Crystal Violet, Eriochrome Black T, and Methyl Orange Dyes onto Biochar-Derived Date Palm Fronds Waste Produced at Different Pyrolysis Conditions. *Water Air Soil Pollut.* **2020**, *231*, 240. [CrossRef]
5. Lee, J.; Kim, K.; Kwon, E.E. Biochar as a catalyst. *Renew. Sustain. Energy Rev.* **2017**, *77*, 70–79. [CrossRef]
6. Ahmad, M.; Rajapaksha, A.U.; Lim, J.E.; Zhang, M.; Bolan, N.; Mohan, D.; Vithanage, M.; Lee, S.S.; Ok, Y.S. Biochar as a sorbent for contaminant management in soil and water: A review. *Chemosphere* **2014**, *99*, 19–23. [CrossRef] [PubMed]
7. Colmenares, J.C.; Varma, R.S.; Lisowski, P. Sustainable hybrid photocatalysts: Titania immobilized on carbon materials derived from renewable and biodegradable resources. *Green Chem.* **2016**, *18*, 5736–5750. [CrossRef]
8. Tomczyk, A.; Sokołowska, Z.; Boguta, P. Biochar physicochemical properties: Pyrolysis temperature and feedstock kind effects. *Rev. Environ. Sci. Biotechnol.* **2020**, *19*, 191–215. [CrossRef]
9. Qin, C.; Wang, H.; Yuan, X.; Xiong, T.; Zhang, J.; Zhang, J. Understanding structure-performance correlation of biochar materials in environmental remediation and electrochemical devices. *Chem. Eng. J.* **2020**, *382*, 122977. [CrossRef]
10. Faria, P.; Órfão, J.; Pereira, M. Adsorption of anionic and cationic dyes on activated carbons with different surface chemistries. *Water Res.* **2004**, *38*, 2043–2052. [CrossRef]

11. Nakagawa, K.; Namba, A.; Mukai, S.R.; Tamon, H.; Ariyadejwanich, P.; Tanthapanichakoon, W. Adsorption of phenol and reactive dye from aqueous solution on activated carbons derived from solid wastes. *Water Res.* **2004**, *38*, 1791–1798. [CrossRef]
12. Chen, W.; Parette, R.; Zou, J.; Cannon, F.S.; Dempsey, B.A. Arsenic removal by iron-modified activated carbon. *Water Res.* **2007**, *41*, 1851–1858. [CrossRef] [PubMed]
13. Ahmad, M.; Lee, S.S.; Dou, X.M.; Mohan, D.; Sung, J.-K.; Yang, J.E.; Ok, Y.S. Effects of pyrolysis temperature on soybean stover- and peanut shell-derived biochar properties and TCE adsorption in water. *Bioresour. Technol.* **2012**, *118*, 536–544. [CrossRef] [PubMed]
14. Lu, H.; Zhang, W.; Yang, Y.; Huang, X.; Wang, S.; Qiu, R. Relative distribution of Pb^{2+} sorption mechanisms by sludge-derived biochar. *Water Res.* **2012**, *46*, 854–862. [CrossRef]
15. Cao, X.; Ma, L.; Gao, B.; Harris, W. Dairy-manure derived biochar effectively sorbs lead and atrazine. *Environ. Sci. Technol.* **2009**, *43*, 3285–3291. [CrossRef]
16. Tan, X.; Liu, Y.; Zeng, G.; Wang, X.; Hu, X.; Gu, Y.; Yang, Z. Application of biochar for the removal of pollutants from aqueous solutions. *Chemosphere* **2015**, *125*, 70–85. [CrossRef]
17. Tsai, C.-Y.; Lin, P.-Y.; Hsieh, S.-L.; Kirankumar, R.; Patel, A.K.; Singhania, R.-R.; Dong, C.-D.; Chen, C.-W.; Hsieh, S. Engineered mesoporous biochar derived from rice husk for efficient removal of malachite green from wastewaters. *Bioresour. Technol.* **2022**, *347*, 126749. [CrossRef]
18. Guo, Z.; Chen, R.; Yang, R.; Yang, F.; Chen, J.; Li, Y.; Zhou, R.; Xu, J. Synthesis of amino-functionalized biochar/spinel ferrite magnetic composites for low-cost and efficient elimination of Ni(II) from wastewater. *Sci. Total. Environ.* **2020**, *722*, 137822. [CrossRef] [PubMed]
19. Xu, Y.; Chen, B. Organic carbon and inorganic silicon speciation in rice-bran-derived biochars affect its capacity to adsorb cadmium in solution. *J. Soils Sediments* **2015**, *15*, 60–70. [CrossRef]
20. Silvia, E.-C.; Valeria, A.-G.; MÁngeles, S.; Marta, P. Eco-approach for pharmaceutical removal: Thermochemical waste valorisation, biochar adsorption and electro-assisted regeneration. *Electrochim. Acta* **2021**, *389*, 138694.
21. Yadav, T.P.; Yadav, R.M.; Singh, D. Mechanical Milling: A Top Down Approach for the Synthesis of Nanomaterials and Nanocomposites. *Nanosci. Nanotechnol.* **2012**, *2*, 22–48. [CrossRef]
22. Naghdi, M.; Taheran, M.; Brar, S.K.; Rouissi, T.; Verma, M.; Surampalli, R.Y.; Valero, J.R. A green method for production of nanobiochar by ball milling-optimization and characterization. *J. Clean. Prod.* **2017**, *164*, 1394–1405. [CrossRef]
23. Feng, K.; Xu, Z.; Gao, B.; Xu, X.; Zhao, L.; Qiu, H.; Cao, X. Mesoporous ball-milling iron-loaded biochar for enhanced sorption of reactive red: Performance and mechanisms. *Environ. Pollut.* **2021**, *290*, 117992. [CrossRef] [PubMed]
24. Yang, G.; Wang, Z.; Xian, Q.; Shen, F.; Sun, C.; Zhang, Y.; Wu, J. Effects of pyrolysis temperature on the physicochemical properties of biochar derived from vermicompost and its potential use as an environmental amendment. *RSC Adv.* **2015**, *5*, 40117–40125. [CrossRef]
25. Huang, H.; Reddy, N.G.; Huang, X.; Chen, P.; Wang, P.; Zhang, Y.; Huang, Y.; Lin, P.; Garg, A. Effects of pyrolysis temperature, feedstock type and compaction on water retention of biochar amended soil. *Sci. Rep.* **2021**, *11*, 7419. [CrossRef]
26. Singha, S.V.; Chaturvedia, S.; Dhyania, V.C.; Kasivelub, G. Pyrolysis temperature influences the characteristics of rice straw and husk biochar and sorption/desorption behavior of their biourea composite. *Bioresour. Technol.* **2020**, *314*, 123674. [CrossRef]
27. Hou, M.-F.; Ma, C.-X.; Zhang, W.-D.; Tang, X.-Y.; Fan, Y.-N.; Wan, H.-F. Removal of rhodamine B using iron-pillared bentonite. *J. Hazard. Mater.* **2011**, *186*, 1118–1123. [CrossRef]
28. Chan, S.-L.; Tan, Y.P.; Abdullah, A.H.; Ong, S.-T. Equilibrium, kinetic and thermodynamic studies of a new potential biosorbent for the removal of Basic Blue 3 and Congo Red dyes: Pineapple (*Ananas comosus*) plant stem. *J. Taiwan Inst. Chem. Eng.* **2016**, *61*, 306–315. [CrossRef]
29. Shaikh, W.A.; Chakraborty, S.; Islam, R.U. Photocatalytic degradation of rhodamine B under UV irradiation using Shorea robusta leaf extract-mediated bio-synthesized silver nanoparticles. *Int. J. Environ. Sci. Technol.* **2020**, *17*, 2059–2072. [CrossRef]
30. Shaikh, W.A.; Alam, A.; Alam, O.; Chakraborty, S.; Owens, G.; Bhattacharya, T.; Mondal, N.K. Enhanced aqueous phase arsenic removal by a biochar based iron nanocomposite. *Environ. Technol. Innov.* **2020**, *19*, 100936. [CrossRef]
31. Han, Y.; Li, W.; Zhang, J.; Meng, H.; Xu, Y.; Zhang, X. Adsorption behavior of Rhodamine B on nanoporous polymers. *RSC Adv.* **2015**, *5*, 104915–104922. [CrossRef]
32. Anstey, A.; Vivekanandhan, S.; Rodriguez-Uribe, A.; Misra, M.; Mohanty, A.K. Oxidative acid treatment and characterization of new biocarbon from sustainable Miscanthus biomass. *Sci. Total. Environ.* **2016**, *550*, 241–247. [CrossRef]
33. Shan, X.; Guo, X.; Yin, Y.; Miao, Y.; Dong, H. Surface modification of graphene oxide by goethite with enhanced tylosin photocatalytic activity under visible light irradiation. *Colloids Surfaces A Physicochem. Eng. Asp.* **2017**, *520*, 420–427. [CrossRef]
34. Azargohar, R.; Nanda, S.; Kozinski, J.A.; Dalai, A.K.; Sutarto, R. Effects of temperature on the physicochemical characteristics of fast pyrolysis bio-chars derived from Canadian waste biomass. *Fuel* **2014**, *125*, 90–100. [CrossRef]

35. Xiang, W.; Wan, Y.; Zhang, X.; Tan, Z.; Xia, T.; Zheng, Y.; Gao, B. Adsorption of tetracycline hydrochloride onto ball-milled biochar: Governing factors and mechanisms. *Chemosphere* **2020**, *255*, 127057. [CrossRef]
36. Skoglund, S.; Hedberg, J.; Yunda, E.; Godymchuk, A.; Blomberg, E.; Wallinder, I.O. Difficulties and flaws in performing accurate determinations of zeta potentials of metal nanoparticles in complex solutions—Four case studies. *PLoS ONE* **2017**, *12*, e0181735. [CrossRef]